Clinical Imaging 39 (2015) 390–395

Primary central nervous system lymphoma and glioblastoma: differentiation using dynamic susceptibility-contrast perfusion-weighted imaging, diffusion-weighted imaging, and ^{18}F-fluorodeoxyglucose positron emission tomography

Satoshi Nakajima, MD[1], Tomohisa Okada, MD, PhD[1], Akira Yamamoto, MD, PhD[1], Mitsunori Kanagaki, MD, PhD[1], Yasutaka Fushimi, MD, PhD[1], Tsutomu Okada, MD, PhD[1], Yoshiki Arakawa, MD, PhD[2], Yasushi Takagi, MD, PhD[2], Susumu Miyamoto, MD, PhD[2], and Kaori Togashi, MD, PhD[1]

[1]Department of Diagnostic Imaging and Nuclear Medicine and [2]Department of Neurosurgery, Kyoto University Graduate School of Medicine, Kyoto, 606-8507 JAPAN.

Abstract

Objective: To evaluate diagnostic performance of dynamic susceptibility-contrast perfusion-weighted imaging, diffusion-weighted imaging, and ^{18}F-fluorodeoxyglucose positron emission tomography in differentiating primary central nervous system lymphoma (PCNSL) and glioblastoma.

Materials and Methods: Twenty-three glioblastomas and 11 PCNSLs were analyzed with uncorrected cerebral blood volume (CBV) ratio, fifth percentile value of cumulative apparent diffusion coefficient histogram ($ADC_{5\%}$), and maximum standardized uptake value (SUV_{max}) using regions of interest created semi-automatically on enhancing areas.

Results: Uncorrected CBV ratio was highly capable of differentiating PCNSL from glioblastoma as well as SUV_{max} and $ADC_{5\%}$.

Conclusions: Uncorrected CBV ratio demonstrates high diagnostic performance comparable to SUV_{max}.

1. Introduction

Primary central nervous system lymphoma (PCNSL) has been increasing over the last few decades in both immunocompetent and immunocompromised patients [1-3], whereas glioblastoma is the most common disorder among the primary central nervous system malignancies [4]. Both tumors usually show contrast enhancement and occasionally have similar features on conventional magnetic resonance (MR) imaging. However, preoperative differentiation between PCNSL and glioblastoma is of high clinical importance, because neurosurgical strategies for these tumors are substantially different. For glioblastoma, maximal resection contributes to better prognosis [5]. In contrast, stereotactic biopsy is recommended to confirm the diagnosis of PCNSL [6].

Previous reports have shown that cerebral blood volume (CBV) derived from dynamic susceptibility-contrast perfusion-weighted MR imaging (DSC-PWI), apparent diffusion coefficient (ADC) on diffusion-weighted MR imaging (DWI) and standardized uptake value (SUV) from ^{18}F-fluorodeoxyglucose positron emission tomography (FDG-PET) are capable of discriminating PCNSL from glioblastoma [7-14]. However, according to several earlier studies, FDG-PET may be superior to DWI [15, 16].

Meanwhile in DSC-PWI, Toh et al. [17] recently reported superiority of uncorrected CBV ratio to corrected CBV ratio in differentiating between PCNSL and glioblastoma. To our knowledge, there has been no report that compared the diagnostic performance

between DSC-PWI and FDG-PET to differentiate the two tumors. Therefore, the purpose of this study was to evaluate the diagnostic performance of uncorrected CBV ratio compared with that of SUV as well as ADC for distinguishing between PCNSL and glioblastoma.

2. Materials and methods

2.1. Patients

The institutional database was searched between December 2010 and June 2014 to identify newly diagnosed and histologically confirmed patients of PCNSL or glioblastoma. Immunocompetent patients who had all of DSC-PWI, DWI and FDG-PET exams preoperatively were included. Excluded from this study were patients who underwent continued steroid therapy or had received steroid-pulse treatment [14]. This retrospective study was approved by the institutional review board, and informed consent was waived.

2.2. MR imaging

MR scans were performed using a 3T unit (Magnetom Trio; Siemens, Erlangen, Germany) equipped with a 32-channel head coil. Routine MR imaging included axial

fast spin-echo T2-weighted imaging (T2WI) (time of repetition [TR], 3200 ms; time of echo [TE], 79 ms; field of view [FOV], 22 cm; matrix size, 448 × 372; slice thickness, 3 mm; slice gap, 1 mm; 35–37 slices) and three-dimensional magnetization-prepared rapid acquisition gradient-echo (MPRAGE) T1-weighted imaging (T1WI) (TR, 1900 ms; TE, 2.58 ms; inversion time, 900 ms; FOV, 23 × 23 cm; matrix size, 256 × 256; slice thickness, 0.9 mm) before and after contrast agent administration.

DWI was obtained in the axial plane using a single-shot spin-echo echo-planar sequence with the following parameters: TR, 5000 ms; TE, 77 ms; flip angle, 90°; FOV, 22 × 22 cm; matrix size, 160 × 160; slice thickness, 3 mm; slice gap, 1 mm; 35–37 slices. Motion probing gradients were applied sequentially in the *x*, *y* and *z* directions with *b* values of 0 and 1000 s/mm^2. ADC maps were generated automatically by the MR unit.

DSC-PWI was acquired with gradient-echo echo-planar imaging by using the following parameters: TR, 2000 ms; TE, 30 ms; flip angle, 90°; FOV, 22 cm; matrix size, 160 × 160; slice thickness, 3 mm; slice gap, 1 mm; 25 slices. Sixty-five dynamic measurements were conducted, resulting in a total acquisition time of 2 minutes 10 seconds. After 25 scans of baseline, a gadolinium-based contrast agent (0.1 ml/kg) was injected intravenously at a rate of 3 ml/s followed by a bolus injection of 15 ml saline at the same rate. No contrast agent was administered before DSC-PWI.

2.3. FDG-PET

FDG-PET studies were performed using a PET/CT scanner (Discovery ST Elite; GE Healthcare, Waukesha, WI, USA). Patients fasted for at least 4 hours prior to the intravenous administration of 4 MBq/kg of FDG, and rested for 30 minutes before scanning. An emission scan of the brain was conducted for 15 minutes. The resolution was 2.0 × 2.0 × 4.25 mm (47 slices). PET data were converted to SUV images using the following equation: SUV = activity at a pixel (kBq/cm^3)/injection dose (MBq)/weight (kg).

2.4. Image analysis

DSC-PWI data were transferred to an independent workstation and processed using commercially available software (MIStar; Apollo Medical Imaging Technology, Melbourne, Australia). The analysis of signal–time course data gives us valuable information including CBV that is considered to reflect microvessel density [7-9]. Uncorrected and corrected CBV were measured on the DSC images by using a model proposed by Boxerman et al. [18], but only uncorrected CBV maps were used because of superiority of uncorrected CBV to corrected CBV in differentiating between PCNSL and glioblastoma [17].

The first DSC image volume was co-registered to the T2WI volume with SPM8 (http://www.fil.ion.ucl.ac.uk/spm/software/spm8/) implemented on Matlab 2013b

(MathWorks, Natick, MA), and the derived registration parameters were applied to the uncorrected CBV map. Pre- and post-contrast T1WI volumes were co-registered to the T2WI volume, and axially reformatted. Pre-contrast T1WI was subtracted from post-contrast T1WI, and a T1-weighted subtraction map was created for a region of interest (ROI) analysis [19]. An ADC map and an SUV image volume were also separately co-registered to the T2WI volume.

ROIs were placed using ImageJ (ver. 1.48; http://imagej.nih.gov/ij/index.html). On a T1-weighted subtraction map, enhancing areas of the tumor were automatically selected by Huang's fuzzy thresholding method [20]. Vessels continuous to the tumor at the edges were manually eliminated, and ROIs were created. Among tumor-containing slices, the single slice with the largest enhancing area was used for further analysis.

The ROIs were applied to the uncorrected CBV maps, and the mean ROI values were obtained [17]. For normalization, the mean uncorrected CBV values were divided by the mean values obtained from a ROI (size range, 30–50 mm^2) placed in the contralateral normal-appearing white matter, which yielded uncorrected CBV ratios. The same ROIs were applied to the ADC maps and SUV images. Cumulative ADC histograms were obtained, and multiple possible thresholds of the Nth percentile from the first to 20th percentile were derived and compared using areas under the curve (AUCs) determined by receiver operating characteristic (ROC) curve analysis for each percentile. The optimal percentile of cumulative ADC histogram which had the largest AUC value was selected [21]. For SUV images, the maximum SUV (SUV_{max}) was

obtained [12]. In addition, the maximum SUV at the whole tumor ($SUV_{max\ (whole)}$) was also obtained.

2.5. Statistical analysis

A Mann-Whitney *U* test was used to compare uncorrected CBV ratio, the optimal percentile of cumulative ADC histogram, and SUV_{max} between PCNSL and glioblastoma. AUCs and optimal cut-off values for tumor differentiation were determined by ROC curve analysis. The optimal cut-off values were decided using Youden index. Additionally, $SUV_{max\ (whole)}$ was analyzed using a Mann-Whitney *U* test and ROC curve analysis. A *P* value of less than .05 was considered statistically significant. A commercially available statistical software package (MedCalc, Version 13.3; MedCalc Software, Ostend, Belgium) was used for statistical analysis.

3. Results

3.1. Patients

Seventy newly diagnosed patients (29 PCNSLs and 41 glioblastomas) were identified in the institutional database, and preoperative DSC-PWI, DWI and FDG-PET data were available in 14 PCNSLs and 23 glioblastomas. Three PCNSL cases were

excluded because of steroid treatment. Thereby, 11 patients with PCNSL (4 men and 7 women; mean age, 70.0 years; range, 39–79 years) and 23 patients with glioblastoma (13 men and 10 women; mean age, 56.5 years; range, 16–90 years) were analyzed in this study. All PCNSLs were diffuse large B cell lymphomas. The mean time interval between MR imaging and FDG-PET was 4.5 days (range, 0–11 days).

3.2. Diagnostic performance

Figure 1 demonstrates the 4th and 5th percentiles have the largest AUC value of cumulative ADC histogram, and the 5th percentile ($ADC_{5\%}$) was selected as with the former study [21]. Figure 2 shows box-and-whisker plots of uncorrected CBV ratio, $ADC_{5\%}$ and SUV_{max} in patients with PCNSL and glioblastoma. Median uncorrected CBV ratio was significantly lower in PCNSL (1.57 ± 0.56; 95% CI, 1.11–1.98; range, 0.86–2.59) than in glioblastoma (4.99 ± 2.89; 95% CI, 2.69–6.27; range, 0.99–10.28) (P = .0001). Median $ADC_{5\%}$ was significantly lower in PCNSL ($0.56 \pm 0.08 \times 10^{-3}$ mm^2/s; 95% CI, $0.50–0.63 \times 10^{-3}$ mm^2/s; range, $0.42–0.68 \times 10^{-3}$ mm^2/s) than in glioblastoma ($0.77 \pm 0.15 \times 10^{-3}$ mm^2/s; 95% CI, $0.69–0.84 \times 10^{-3}$ mm^2/s; range, $0.53–1.08 \times 10^{-3}$ mm^2/s) (P = .0003). Median SUV_{max} was significantly higher in PCNSL (15.8 ± 6.4; 95% CI, 11.1–20.4; range, 9.4–30.9) than in glioblastoma (7.9 ± 2.8; 95% CI, 6.1–9.1; range, 4.3–15.7) (P = .0001).

In ROC curve analysis, the optimal cut-off value was 2.09 for uncorrected CBV

ratio with 90.9% sensitivity and 91.3% specificity. For $ADC_{5\%}$, the optimal cut-off value was 0.68×10^{-3} mm^2/s with 100% sensitivity and 73.9% specificity. For SUV_{max}, the optimal cut-off value was 9.35 with 100% sensitivity and 78.3% specificity. The AUCs were 0.921 for uncorrected CBV ratio, 0.885 for $ADC_{5\%}$ and 0.933 for SUV_{max}. There was no significant difference in diagnostic performance among these parameters. Figures 3 and 4 illustrate measurements in representative cases of PCNSL and glioblastoma, respectively.

Median $SUV_{max\ (whole)}$ was significantly higher in PCNSL (17.0 ± 6.9; 95% CI, 12.2–21.6; range, 9.4–34.1) than in glioblastoma (8.9 ± 3.5; 95% CI, 7.0–9.6; range, 4.7–20.1) (P = .0001). In ROC curve analysis, the optimal cut-off value was 11.1 for $SUV_{max\ (whole)}$ with 90.9% sensitivity and 87.0% specificity, and the AUC was 0.925. There was no significant difference in diagnostic performance between SUV_{max} and $SUV_{max\ (whole)}$ (P = .700).

4. Discussion

This study evaluated the diagnostic performance of DSC-PWI, DWI and FDG-PET to differentiate PCNSL from glioblastoma. To our knowledge, this is the first report to compare the diagnostic performance between two different modalities of DSC-PWI and FDG-PET in distinguishing these tumors. ROIs were created semi-automatically by thresholding, and the same ROIs were applied to all measurements. In the present study,

PCNSL demonstrated significantly lower uncorrected CBV ratio, lower $ADC_{5\%}$ and higher SUV_{max} compared with glioblastoma. No significant difference in diagnostic performance was observed among these parameters.

SUV derived from FDG-PET is known to represent glucose metabolism in tumors, and high SUV is correlated with rapid cellular proliferation [22, 23]. Previous investigations have shown higher SUV_{max} in PCNSL than in glioblastoma [12-16], which was confirmed in this study. The difference between SUV_{max} and $SUV_{max\ (whole)}$ in diagnostic performance was examined, which was not statistically significant. Okada et al. [13] reported that the AUC was 0.935 when the maximum SUV was measured in the entire lesions, and our result was virtually the same.

It has been reported that ADC calculated from DWI inversely correlates with tumor cell density [10], and high cellularity of PCNSL is considered to result in low ADC. In the present study, $ADC_{5\%}$ for patients with PCNSL was significantly lower than that for patients with glioblastoma, which is consistent with previous reports [8-11]. However, several previous investigations have considered FDG-PET to be superior to DWI [15, 16]. The AUC of $ADC_{5\%}$ was considerably lower than that of SUV_{max} in this study, but the difference was not statistically significant.

Several previous studies [7-9] have reported that PCNSL demonstrates lower CBV than glioblastoma, which was confirmed in this study. That is considered to reflect their histological changes. PCNSL lacks in prominent neovascularization, but it has characteristic features with angiocentric growth patterns [24-26]. Infiltration into the

endothelium and vessel lumen is often observed [2, 27], which is considered to cause disruption of the blood brain barrier [28]. On the other hand, one of the hallmarks of glioblastoma is extensive tumor angiogenesis [29]. Such histological findings may cause the difference in measured CBV.

DSC-PWI measures T2*-weighted signal-intensity drop occurring over a bolus administration of contrast agent. However, when the blood brain barrier breaks down, contrast agent leaks into the extracellular space, and T2*-weighted signal-intensity reduction is mitigated by the T1 shortening effect, resulting in underestimation of CBV [30]. Toh et al. [17] recently reported that uncorrected CBV ratio was superior to corrected CBV ratio in differentiating PCNSL from glioblastoma. When the measurement is left uncorrected, CBV in PCNSL is underestimated more than that in glioblastoma by the effect of a larger degree of contrast leakage. This effect enabled uncorrected CBV ratio to attain the result comparable to SUV_{max}.

Our study has several limitations. The first one is the retrospective study design. Secondly, the relatively small number of patients was included in the analysis. Lastly, direct correlations between parameters and histological features were unavailable, because tumors were biopsied or resected piece-wise.

In conclusion, DSC-PWI is highly capable of differentiating PCNSL from glioblastoma as well as FDG-PET and DWI, and uncorrected CBV ratio demonstrates high diagnostic performance comparable to SUV_{max}.

References

[1] Olson JE, Janney CA, Rao RD, Cerhan JR, Kurtin PJ, Schiff D, et al. The continuing increase in the incidence of primary central nervous system non-Hodgkin lymphoma: a surveillance, epidemiology, and end results analysis. Cancer. 2002;95:1504-10.

[2] Bhagavathi S, Wilson JD. Primary central nervous system lymphoma. Archives of pathology & laboratory medicine. 2008;132:1830-4.

[3] Raoux D, Duband S, Forest F, Trombert B, Chambonniere ML, Dumollard JM, et al. Primary central nervous system lymphoma: immunohistochemical profile and prognostic significance. Neuropathology : official journal of the Japanese Society of Neuropathology. 2010;30:232-40.

[4] DeAngelis LM. Brain tumors. The New England journal of medicine. 2001;344:114-23.

[5] Giese A, Westphal M. Treatment of malignant glioma: a problem beyond the margins of resection. Journal of cancer research and clinical oncology. 2001;127:217-25.

[6] Schultz CJ, Bovi J. Current management of primary central nervous system lymphoma. International journal of radiation oncology, biology, physics. 2010;76:666-78.

[7] Hartmann M, Heiland S, Harting I, Tronnier VM, Sommer C, Ludwig R, et al. Distinguishing of primary cerebral lymphoma from high-grade glioma with

perfusion-weighted magnetic resonance imaging. Neuroscience letters. 2003;338:119-22.

[8] Calli C, Kitis O, Yunten N, Yurtseven T, Islekel S, Akalin T. Perfusion and diffusion MR imaging in enhancing malignant cerebral tumors. European journal of radiology. 2006;58:394-403.

[9] Kickingereder P, Wiestler B, Sahm F, Heiland S, Roethke M, Schlemmer HP, et al. Primary Central Nervous System Lymphoma and Atypical Glioblastoma: Multiparametric Differentiation by Using Diffusion-, Perfusion-, and Susceptibility-weighted MR Imaging. Radiology. 2014;272:843-50.

[10] Guo AC, Cummings TJ, Dash RC, Provenzale JM. Lymphomas and high-grade astrocytomas: comparison of water diffusibility and histologic characteristics. Radiology. 2002;224:177-83.

[11] Doskaliyev A, Yamasaki F, Ohtaki M, Kajiwara Y, Takeshima Y, Watanabe Y, et al. Lymphomas and glioblastomas: differences in the apparent diffusion coefficient evaluated with high b-value diffusion-weighted magnetic resonance imaging at 3T. European journal of radiology. 2012;81:339-44.

[12] Kosaka N, Tsuchida T, Uematsu H, Kimura H, Okazawa H, Itoh H. 18F-FDG PET of common enhancing malignant brain tumors. AJR American journal of roentgenology. 2008;190:W365-9.

[13] Okada Y, Nihashi T, Fujii M, Kato K, Okochi Y, Ando Y, et al. Differentiation of newly diagnosed glioblastoma multiforme and intracranial diffuse large B-cell

Lymphoma using (11)C-methionine and (18)F-FDG PET. Clinical nuclear medicine. 2012;37:843-9.

[14] Yamaguchi S, Hirata K, Kobayashi H, Shiga T, Manabe O, Kobayashi K, et al. The diagnostic role of (18)F-FDG PET for primary central nervous system lymphoma. Annals of nuclear medicine. 2014;28:603-9.

[15] Makino K, Hirai T, Nakamura H, Murakami R, Kitajima M, Shigematsu Y, et al. Does adding FDG-PET to MRI improve the differentiation between primary cerebral lymphoma and glioblastoma? Observer performance study. Annals of nuclear medicine. 2011;25:432-8.

[16] Matsushima N, Maeda M, Umino M, Suzawa N, Yamada T, Takeda K. Relation between FDG uptake and apparent diffusion coefficients in glioma and malignant lymphoma. Annals of nuclear medicine. 2012;26:262-71.

[17] Toh CH, Wei KC, Chang CN, Ng SH, Wong HF. Differentiation of primary central nervous system lymphomas and glioblastomas: comparisons of diagnostic performance of dynamic susceptibility contrast-enhanced perfusion MR imaging without and with contrast-leakage correction. AJNR American journal of neuroradiology. 2013;34:1145-9.

[18] Boxerman JL, Schmainda KM, Weisskoff RM. Relative cerebral blood volume maps corrected for contrast agent extravasation significantly correlate with glioma tumor grade, whereas uncorrected maps do not. AJNR American journal of neuroradiology. 2006;27:859-67.

[19] Ellingson BM, Kim HJ, Woodworth DC, Pope WB, Cloughesy JN, Harris RJ, et al. Recurrent glioblastoma treated with bevacizumab: contrast-enhanced T1-weighted subtraction maps improve tumor delineation and aid prediction of survival in a multicenter clinical trial. Radiology. 2014;271:200-10.

[20] Huang LK, Wang MJJ. Image Thresholding by Minimizing the Measures of Fuzziness. Pattern Recogn. 1995;28:41-51.

[21] Chu HH, Choi SH, Ryoo I, Kim SC, Yeom JA, Shin H, et al. Differentiation of true progression from pseudoprogression in glioblastoma treated with radiation therapy and concomitant temozolomide: comparison study of standard and high-b-value diffusion-weighted imaging. Radiology. 2013;269:831-40.

[22] Rosenfeld SS, Hoffman JM, Coleman RE, Glantz MJ, Hanson MW, Schold SC. Studies of primary central nervous system lymphoma with fluorine-18-fluorodeoxyglucose positron emission tomography. Journal of nuclear medicine : official publication, Society of Nuclear Medicine. 1992;33:532-6.

[23] Benard F, Romsa J, Hustinx R. Imaging gliomas with positron emission tomography and single-photon emission computed tomography. Seminars in nuclear medicine. 2003;33:148-62.

[24] Koeller KK, Smirniotopoulos JG, Jones RV. Primary central nervous system lymphoma: radiologic-pathologic correlation. Radiographics : a review publication of the Radiological Society of North America, Inc. 1997;17:1497-526.

[25] Kadoch C, Treseler P, Rubenstein JL. Molecular pathogenesis of primary central

nervous system lymphoma. Neurosurgical focus. 2006;21:E1.

[26] Louis DN, Ohgaki H, Wiestler OD, Cavenee WK. Malignant lymphomas. In: Deckert M, Paulus W, editors. WHO Classification of Tumours of the Central Nervous System, Fourth Edition. Lyon, France: IARC Press; 2007. p. 188-92.

[27] Molnar PP, O'Neill BP, Scheithauer BW, Groothuis DR. The blood-brain barrier in primary CNS lymphomas: ultrastructural evidence of endothelial cell death. Neuro-oncology. 1999;1:89-100.

[28] Watanabe M, Tanaka R, Takeda N, Wakabayashi K, Takahashi H. Correlation of computed tomography with the histopathology of primary malignant lymphoma of the brain. Neuroradiology. 1992;34:36-42.

[29] Wesseling P, Ruiter DJ, Burger PC. Angiogenesis in brain tumors; pathobiological and clinical aspects. Journal of neuro-oncology. 1997;32:253-65.

[30] Willats L, Calamante F. The 39 steps: evading error and deciphering the secrets for accurate dynamic susceptibility contrast MRI. NMR in biomedicine. 2013;26:913-31.

Figures

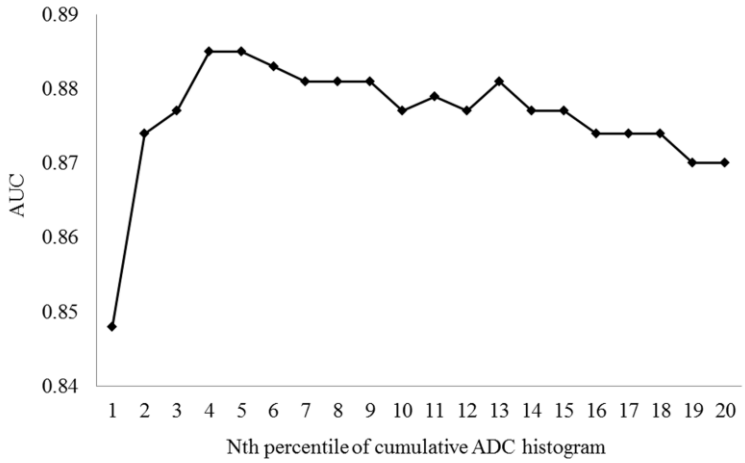

Fig. 1. Measurements of areas under ROC curve at multiple Nth percentiles (from the first to 20th percentile) of cumulative ADC histogram. The 4th and 5th percentiles have the largest AUC value.

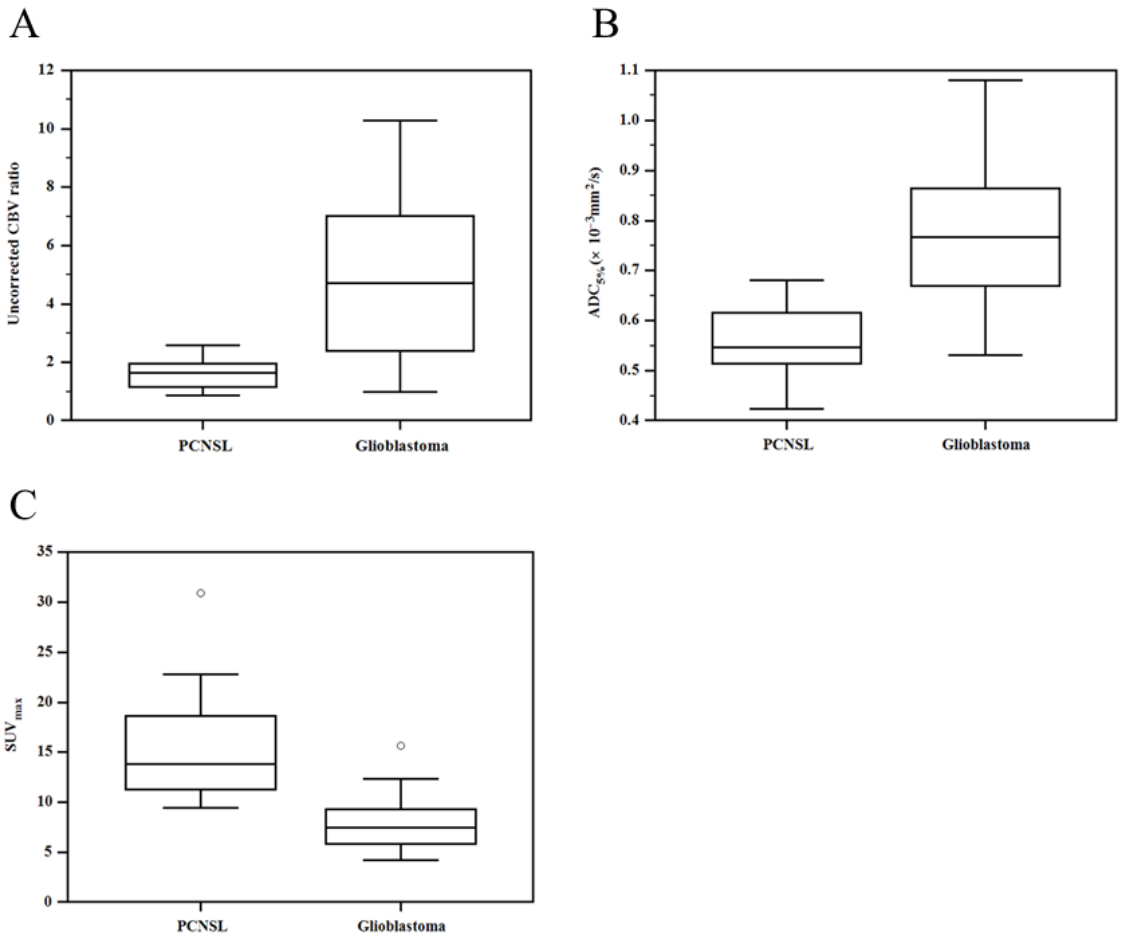

Fig. 2. Box-and-whisker plots of uncorrected CBV ratio (A), $ADC_{5\%}$ (B), and SUV_{max} (C) for PCNSL and glioblastoma. The central boxes represent the values from the lower to upper quartile (25th to 75th percentile). The middle lines represent the median. The vertical lines on each box indicate the range of data distribution. Values outside of 1.5 times of the interquartile range are presented with open circles.

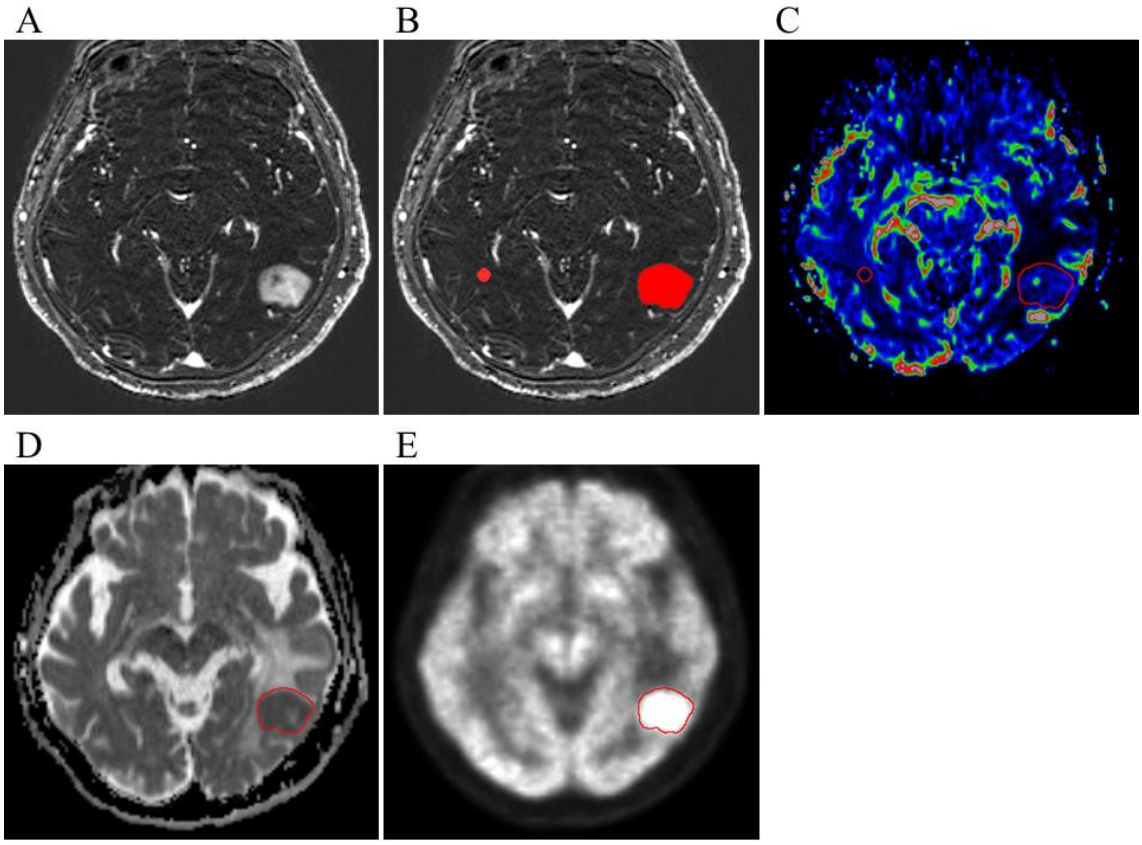

Fig. 3. Measurements of parameters in a 77-year-old woman with PCNSL. (A) Axial T1-weighted subtraction map shows an enhancing tumor in the left temporal region. (B) Two ROIs are placed, one over the enhancing tumor and the other at the contralateral normal-appearing white matter for the measurement of (C) uncorrected CBV ratio, (D) $ADC_{5\%}$, and (E) SUV_{max} with values of 1.96, 0.54×10^{-3} mm^2/s, and 11.14, respectively.

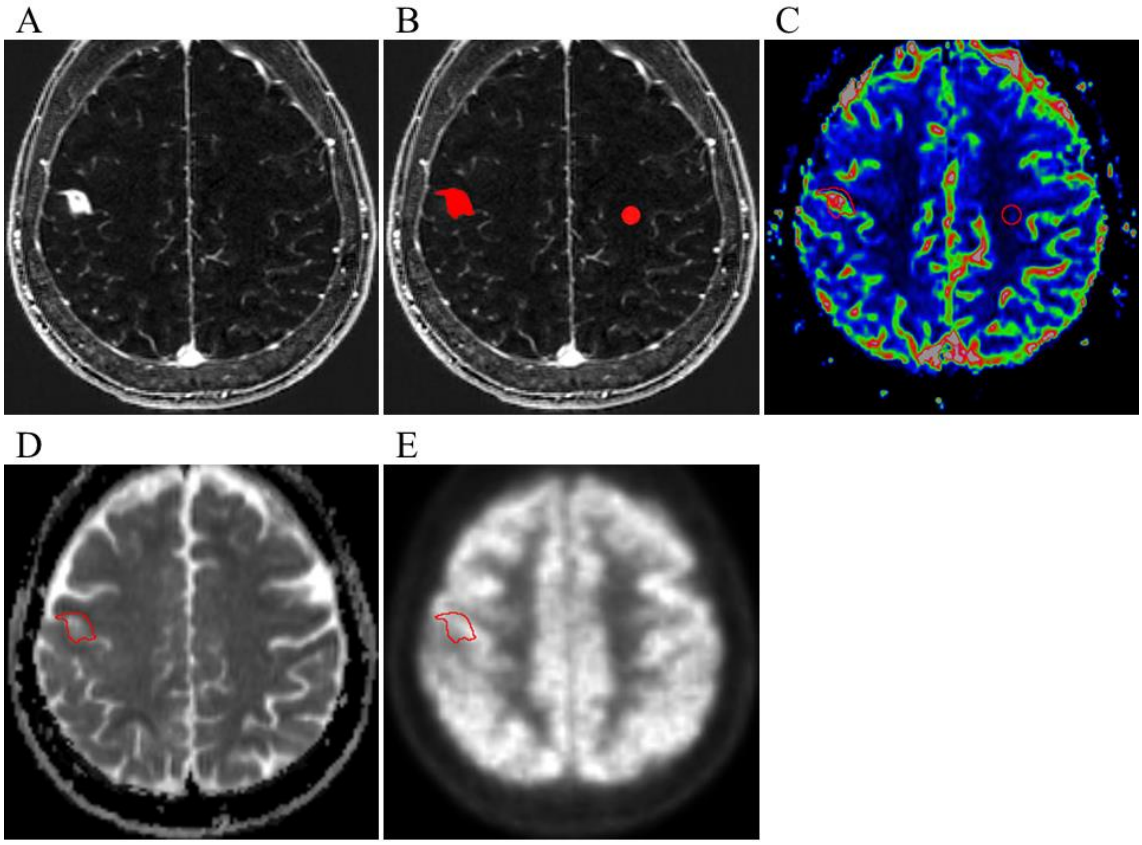

Fig. 4. Measurements of parameters in a 56-year-old woman with glioblastoma. (A) Axial T1-weighted subtraction map shows an enhancing tumor in the right parietal region. (B) Two ROIs are placed, one over the enhancing tumor and the other at the contralateral normal-appearing white matter for the measurement of (C) uncorrected CBV ratio, (D) $ADC_{5\%}$, and (E) SUV_{max} with values of 7.23, 0.69×10^{-3} mm^2/s, and 7.49, respectively.